Shape evolution in the neutron-rich osmium isotopes: Prompt γ-ray spectroscopy of 196Os

P. R. John,[1,2,*] V. Modamio,[3] J. J. Valiente-Dobón,[3] D. Mengoni,[1,2] S. Lunardi,[1,2] T. R. Rodríguez,[4,5] D. Bazzacco,[2] A. Gadea,[6] C. Wheldon,[7] T. Alexander,[8] G. de Angelis,[3] N. Ashwood,[7] M. Barr,[7] G. Benzoni,[9,10] B. Birkenbach,[11] P. G. Bizzeti,[12,13] A. M. Bizzeti-Sona,[12,13] S. Bottoni,[9,10] M. Bowry,[8] A. Bracco,[9,10] F. Browne,[14] M. Bunce,[8] F. Camera,[9,10] B. Cederwall,[15] L. Corradi,[3] F. C. L. Crespi,[9,10] P. Désesquelles,[16] J. Eberth,[11] E. Farnea,[2,†] E. Fioretto,[3] A. Görgen,[17,18] A. Gottardo,[1,3] J. Grebosz,[19] L. Grente,[17] H. Hess,[11] A. Jungclaus,[20] Tz. Kokalova,[7] A. Korichi,[16] W. Korten,[17] A. Kuşoğlu,[21] S. Lenzi,[1,2] S. Leoni,[9,10] J. Ljungvall,[16] G. Maron,[3] W. Meczynski,[19] B. Melon,[12,13] R. Menegazzo,[1,2] C. Michelagnoli,[1,2,‡] T. Mijatović,[22] B. Million,[10] P. Molini,[1,2] G. Montagnoli,[1,2] D. Montanari,[1,2,§] D. R. Napoli,[3] P. Nolan,[23] Ch. Oziol,[24] Zs. Podolyák,[8] G. Pollarolo,[25,26] A. Pullia,[9,10] B. Quintana,[27] F. Recchia,[1,2] P. Reiter,[11] O. J. Roberts,[14] D. Rosso,[3] E. Şahin,[3,¶] M.-D. Salsac,[17] F. Scarlassara,[1,2] M. Sferrazza,[28] J. Simpson,[29] P.-A. Söderström,[30,‖] A. M. Stefanini,[3] O. Stezowski,[31] S. Szilner,[22] Ch. Theisen,[17] C. A. Ur,[2,#] and J. Walshe[7]

[1]*Dipartimento di Fisica e Astronomia, Università di Padova, I-35131 Padova, Italy*
[2]*Istituto Nazionale di Fisica Nucleare, Sezione di Padova, I-35131 Padova, Italy*
[3]*Istituto Nazionale di Fisica Nucleare, Laboratori Nazionali di Legnaro, I-35020 Legnaro, Italy*
[4]*Institut für Kernphysik, Technische Universität Darmstadt, D-64289 Darmstadt, Germany*
[5]*Departamento de Física Teórica, Universidad Autónoma de Madrid, E-28049 Madrid, Spain*
[6]*Instituto de Física Corpuscular, CSIC-Universitat de València, E-46980 València, Spain*
[7]*School of Physics and Astronomy, University of Birmingham, Edgbaston, Birmingham B15 2TT, United Kingdom*
[8]*Department of Physics, University of Surrey, GU2 7XH Guildford, United Kingdom*
[9]*Dipartimento di Fisica, Università di Milano, I-20133 Milano, Italy*
[10]*Istituto Nazionale di Fisica Nucleare, Sezione di Milano, I-20133 Milano, Italy*
[11]*Institut für Kernphysik, Universität zu Köln, D-50937 Köln, Germany*
[12]*Dipartimento di Fisica, Università di Firenze, I-50019 Sesto Fiorentino (Firenze), Italy*
[13]*Istituto Nazionale di Fisica Nucleare, Sezione di Firenze, I-50019 Sesto Fiorentino (Firenze), Italy*
[14]*School of Computing, Engineering and Mathematics, University of Brighton, Brighton BN2 4GJ, United Kingdom*
[15]*Department of Physics, Royal Institute of Technology, SE-10691 Stockholm, Sweden*
[16]*Centre de Spectrométrie Nucléaire et de Spectrométrie de Masse CSNSM, CNRS/IN2P3 and Université Paris-Sud, F-91405 Orsay Campus, France*
[17]*Institut de Recherche sur les lois Fondamentales de l'Univers IRFU, CEA/DSM, Centre CEA de Saclay, F-91191 Gif-sur-Yvette Cedex, France*
[18]*Department of Physics, University of Oslo, N-0316 Oslo, Norway*
[19]*The Henryk Niewodniczański Institute of Nuclear Physics, Polish Academy of Sciences, 31-342 Kraków, Poland*
[20]*Instituto de Estructura de la Materia, CSIC, Madrid, E-28006 Madrid, Spain*
[21]*Department of Physics, Faculty of Science, Istanbul University, Vezneciler/Fatih, TR-34134, İstanbul, Turkey*
[22]*Institut Ruđer Bošković, HR-10000 Zagreb, Croatia*
[23]*Oliver Lodge Laboratory, The University of Liverpool, Liverpool, L69 7ZE, United Kingdom*
[24]*Institut de Physique Nucléaire d'Orsay - IPNO, CNRS/IN2P3 and Université Paris-Sud, F-91406 Orsay Campus, France*
[25]*Dipartimento di Fisica Teorica, Università di Torino, I-10125 Torino, Italy*
[26]*Istituto Nazionale di Fisica Nucleare, Sezione di Torino, I-10125 Torino, Italy*
[27]*Laboratorio de Radiaciones Ionizantes, Universidad de Salamanca, E-37008 Salamanca, Spain*
[28]*Département de Physique, Université libre de Bruxelles, B-1050 Bruxelles, Belgium*
[29]*STFC Daresbury Laboratory, Daresbury, Warrington, WA4 4AD, United Kingdom*
[30]*Department of Physics and Astronomy, Uppsala University, SE-75120 Uppsala, Sweden*
[31]*Université de Lyon, CNRS-IN2P3, Institut de Physique Nucléaire de Lyon, F-69622 Villeurbanne, France*

The shape transition in the neutron-rich Os isotopes is studied by investigating the neutron-rich 196Os nucleus through in-beam γ-ray spectroscopy using a two-proton transfer reaction from a 198Pt target to a 82Se beam. The beam-like recoils were detected and identified with the large-acceptance magnetic spectrometer PRISMA, and the coincident γ rays were measured with the advanced gamma tracking array (AGATA) demonstrator. The de-excitation of the low-lying levels of the yrast-band of 196Os were identified for the first time. The results are compared with state-of-the-art beyond-mean-field calculations, performed for the even-even 188−198Os isotopes. The new results suggest a smooth transition in the Os isotopes from a more axial rotational behavior towards predominately vibrational nuclei through triaxial configurations. An almost perfect γ-unstable/triaxial

rotor yrast band is predicted for ^{196}Os which is in agreement with the experimentally measured excited states.

The equilibrium shapes that characterize the ground states of atomic nuclei are a unique feature of finite many-body quantum systems, also including atoms and molecules. The existence of non-spherical (deformed) shapes in nuclei represents spontaneous symmetry breaking. Although the intrinsic shape of a nucleus is not directly observable, the low-lying excitations of many atomic nuclei can be understood in simple terms as oscillations and/or rotations of macroscopic objects, characterized by spherical or quadrupole-deformed equilibrium shapes. The comparison between the experimental spectra and the predictions of geometrical models, for example, a vibrator, an axial-symmetric rotor, or a γ-soft/triaxial rotor [1] can reveal the underlying shape of the nucleus. Considering particle-hole symmetry in a very simplified view, the number of prolate- (rugby-ball-) and oblate- (pumpkin-) shaped nuclei in nature would be expected to be approximately equal. However, current knowledge from both theory and experiment is that for deformed nuclei there is an extreme paucity of axial-oblate shapes (see Ref. [2] and references therein). In gaining insight into this effect, the regions in the Segrè chart that exhibit oblate deformation or non-axial symmetry (such as triaxiality) become of extraordinary importance. Answering the question of why prolate shapes predominate requires an understanding of the subtle interplay between single-particle and collective degrees-of-freedom and opens a window on the underlying *NN* interaction and its role in the microscopic origin of deformation.

A particularly interesting region of the chart is centered on the $A \sim 190$ transitional elements because a prolate-to-oblate shape transition has been predicted to occur from the less neutron-rich Pt-Os-W isotopes towards the more neutron-rich as the $N = 126$ closed shell is approached. As a result this region has attracted much theoretical and experimental effort in recent years. From a theoretical point of view mean-field approaches have been used extensively with a variety of interactions [3–6] exposing the relevance of triaxial deformation in these nuclei. Nevertheless, spectroscopic information cannot be extracted from mean-field calculations. To compare with the experimental data, the interacting boson approximation

has been applied so far [7]. However, fully self-consistent beyond-mean-field calculations using the same underlying interaction, which provide spectroscopic information, were still missing in this region and will be discussed in this Rapid Communication. Experimental endeavor has mainly focused on spectroscopy to characterize the shape of the lowest-lying excited states [8–12]. Shape properties can most readily be elucidated by examining changes along isotopic or isotonic chains. In the case of the neutron-rich osmium isotopes ($Z = 76$), experimental information is scarce due to the difficulty, in the past, in populating these heavy nuclei. The progress of contemporary studies using deep-inelastic and relativistic fragmentation reactions make the osmium chain accessible, for which a clear transition to oblate shapes is predicted. The ground states of the lighter osmium isotopes ($A \sim 180$–190) are prolate deformed and sphericity is expected to be restored at the $N = 126$ shell closure. However, the path between these limits has yet to be expounded. The heaviest stable isotope, ^{192}Os, has a prolate $J^{\pi} = 10^{-}$ isomer [13,14], but additionally, its γ-vibrational band is the lowest lying in this region with the bandhead at 489 keV [14], a clear signature of γ softness. On the other hand, ^{194}Os, populated up to $J^{\pi} = (10^{+})$ via a multinucleon transfer reaction [9], has a level scheme suggestive of prolate deformation, at variance with the interpretation of previous experimental results [15]. In recent years, isomer-decay spectroscopy combined with fragmentation reactions at relativistic energies has enabled the study of, for example, ^{198}Os; the most neutron-rich osmium isotope for which any spectroscopic information is available. The (2_1^+) and (4_1^+) states in ^{198}Os were identified following the decay of the (7_1^-) isomer, and a weak oblate deformation was deduced from their excitation energies [11]. Osmium-196 was also produced in the fragmentation reactions; however, no γ rays were observed in coincidence [11,12,16,17]. The reason might be absence of an isomer in this nucleus, or an isomer with a very short or long half-life. Prior to the present study, in the eighties, two excited states in ^{196}Os were established, populated via the two-proton transfer reaction ^{198}Pt(^{14}C,^{16}O)^{196}Os [8]. These states lie at 300 (20) and 760 (20) keV. Whereas the first excited state was assumed to be the 2_1^+ state, for the second excited state a 2_2^+, 4_1^+ or doublet of these two states was suggested. However, up to now, no γ-ray transitions have been measured in ^{196}Os.

In this Rapid Communication, the first measurement of excited states in ^{196}Os through in-beam γ-ray spectroscopy is reported. This was possible by using the binary partner method [18], well suited for these heavy neutron-rich cases, in combination with the new generation advanced gamma tracking array (AGATA) demonstrator [19,20] and the PRISMA [21–23] spectrometer. The newly measured energies of the low-lying excited states, together with those already known in the Os isotopic chain have been compared with state-of-the-art beyond-mean-field calculations. This has allowed us to derive the γ-soft character of these transitional nuclei that undergo a prolate-to-oblate shape transition.

————

*Corresponding author: philipp.john@pd.infn.it

†Deceased.

‡Present address: GANIL, CEA/DSM-CNRS/IN2P3, F-14076, Caen, France.

§Present address: USIAS - Universite de Strasbourg, IPHC-CNRS, F-67037 Strasbourg Cedex 2, France.

¶Present address: Department of Physics, University of Oslo, P. O. Box 1048 Blindern, N-0316 Oslo, Norway.

∥Present address: RIKEN Nishina Center, Wako, 351-0198 Saitama, Japan.

#Present address: Extreme Light Infrastructure - Nuclear Physics Facility, MG-6 Bucharest Magurele, Romania.

Neutron-rich Os isotopes were produced by a multinucleon transfer reaction of a ^{82}Se beam impinging on a 2 mg/cm^2 metallic ^{198}Pt self-supporting target. The target was facing the beam tilted at an angle of 85°, to allow target-like and beam-like recoils to exit the target. The beam was provided by the Tandem-ALPI accelerator complex at the Laboratori Nazionali di Legnaro (LNL), Italy, with an energy of 426 MeV. The intensity was kept between 2 and 3 pnA. The beam-like fragments were detected by the large-acceptance PRISMA spectrometer, placed at the grazing angle of the beam-like recoils (57°) with respect to the beam axis. The settings were optimized for detecting Kr isotopes, the binary partner of Os.

The AGATA demonstrator was used for detecting coincident γ rays. It was placed at a distance of 15.5 cm from the target with an angle of 180° with respect to the optical axis of the PRISMA spectrometer. For this experiment the AGATA demonstrator was equipped with five triple clusters. Each cluster consists of three differently shaped hexagonal tapered coaxial high-purity germanium (HPGe) detectors having 36 outer segments with a common core contact. A 600 μm thick Sn absorber was placed in front of the AGATA detectors to reduce the counting rate in the first segments due to x rays. The solid angle coverage of the AGATA demonstrator was 15% of 4π, while its efficiency after tracking was around 4%. The rate for each crystal was maintained between 20 and 30 kHz during the whole experiment. The trigger selected an ion arriving at the focal plane of PRISMA and at least one AGATA crystal firing. The digitized signals of AGATA for all accepted events were written to disk.

Pulse shape analysis was then applied to the digitized AGATA signals, followed by the reconstruction of the γ rays by passing the energy and position of each interaction to the Orsay forward tracking algorithm (OFT) [24]. The interaction time of each γ ray is deduced from its first interaction point, as reconstructed by the tracking algorithm. The atomic charge number, charge, and mass are uniquely identified in the PRISMA spectrometer. The mass resolution achieved, $\frac{1}{280}$, allows the selection of the beam-like nucleus of interest without any observable contamination.

The prompt-coincidence peak for the time difference between AGATA and PRISMA has a FWHM of 15 ns when selecting only the krypton isotopes. This permits the measurement of delayed γ rays and the half-life of isomeric states with $8 \lesssim T_{1/2} \lesssim 400$ ns. The sensitivity is limited by the resolution of the prompt peak and the acquisition time window.

The Doppler correction for the beam-like ions uses the position information of the first interaction point of the reconstructed γ ray and the entrance position in the PRISMA spectrometer. The velocity vector for the target-like recoils is reconstructed event-by-event using relativistic two-body reaction kinematics assuming a pure binary reaction without any particle evaporation. The energy loss for each recoil and the beam ion is taken into account event-by-event using the Northcliffe-Schilling approximation [25]. A FWHM of 0.61% (4.9 keV) for the $6_1^+ \rightarrow 4_1^+$ transition in ^{198}Pt at 729.1 keV is achieved. The simultaneous measurement of both the momentum and the angle of the beam-like recoils enables a reconstruction of the Q value of the reaction. Due to the relatively thick target, 2 mg/cm^2, and the position
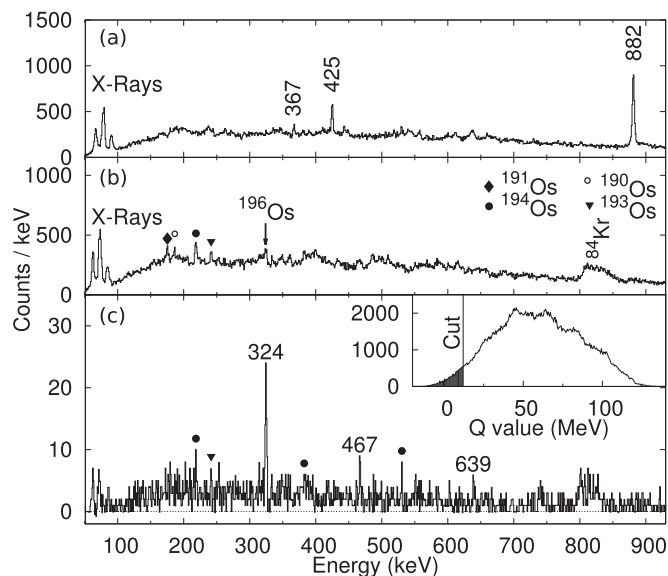

FIG. 1. γ-ray spectra obtained after gating on the beam-like recoils ^{84}Kr. (a) The spectrum is Doppler corrected for ^{84}Kr. The strongest γ ray transitions of ^{84}Kr are labeled. (b) The spectrum is Doppler corrected for ^{196}Os, the binary partner of ^{84}Kr. The wrongly Doppler corrected $2_1^+ \rightarrow 0_{\rm gs}^+$ γ transition of ^{84}Kr and the $(2_1^+) \rightarrow 0_{\rm gs}^+$ of ^{196}Os are indicated. The strongest transitions from other Os isotopes, populated after neutron evaporation, are indicated by different symbols. (c) The same as (b) with an additional gate on the reconstructed Q value <12 MeV (see inset) and a multiplicity of the γ rays of one. Peaks labeled by the energy are assigned to ^{196}Os.

uncertainty of the beam spot on the target, the uncertainty in the reconstructed Q value is around 30 MeV. The deduced mass assuming a true binary reaction only provides an upper limit for the mass of the target-like recoil due to the possible evaporation of neutrons. Therefore, the spectrum gated on the true binary partner of a certain Os isotope also contains transitions from lighter Os isotopes. Figure 1 shows the spectra gated on ^{84}Kr. For the top panel, the Doppler correction is done for ^{84}Kr. In Fig. 1(b), the Doppler correction is performed for ^{196}Os, the binary partner of ^{84}Kr. In this spectrum, transitions from ^{196}Os and from lighter Os isotopes (present due to neutron evaporation) become apparent.

Since an energy greater than the neutron-separation energy needs to be transferred for enabling neutron evaporation, a condition on a low reconstructed Q value suppresses the presence of isotopes with a mass lower than that of the true binary partner. Figure 1(c) shows the γ-ray spectrum Doppler corrected for ^{196}Os, gated on ^{84}Kr and on a reconstructed Q value smaller than 12 MeV with a γ-ray multiplicity of 1. The additional condition on the multiplicity of the reconstructed γ rays produces cleaner spectra. Three γ rays at 324, 467, and 639 keV can be identified in this spectrum. Their relative intensities are reported in Table I. γ rays with such energies are not present in the spectra gated on ^{85}Kr and higher masses (i.e., the binary partner of ^{195}Os and Os isotopes with lower masses). Hence, these three γ rays are all assigned to come from the decay of excited states in ^{196}Os.

TABLE I. Energies E_γ and relative intensities I_γ of the observed γ-ray transitions for ^{196}Os. The intensities are given with a condition on a reconstructed Q value smaller than 12 MeV and only one detected γ ray [$I_{\gamma,M=1,Q<12}$, spectrum Fig. 1(c)] and on a reconstructed Q value smaller than 30 MeV [$I_{\gamma,Q<30}$, spectrum Fig. 2(a) top]. The tentative spin assignment of the transitions and the energy of the level $E(J_i)$ are also given. See text for details.

E_γ (keV)	$I_{\gamma,M=1,Q<12}$	$I_{\gamma,Q<30}$	$J_i^\pi \rightarrow J_f^\pi$	$E(J_i)$ (keV)
324.4 (10)	100 (17)	100 (12)	$(2_1^+) \rightarrow 0_{gs}^+$	324.4
467.0 (10)	31 (11)	41 (10)	$(4_1^+) \rightarrow (2_1^+)$	791.4
639.2 (10)	22 (10)	12 (8)	$(6_1^+) \rightarrow (4_1^+)$	(1430.6)

To verify if the three transitions assigned to ^{196}Os belong to the same decay sequence, a γ-γ matrix in coincidence with ^{84}Kr and a reconstructed Q value smaller than 12 MeV as in Fig. 1 has been produced.

The low statistics prevented the establishment of a clear γ-γ relationship between the three transitions, as expected in view of the quoted AGATA demonstrator efficiency. Therefore, to increase the statistics a γ-γ matrix was built with a reconstructed Q value smaller than 30 MeV, of course at the cost of reducing the peak-to-total ratio [compare Figs. 1(c) and 2(a) upper spectrum]. The results from the γ-γ-coincidence analysis are shown in Fig. 2(a) and reveal that the 324 and 467 keV transitions are in mutual coincidence. On the other hand, the transition at 639 keV does not appear to be in coincidence with any γ-ray transition. On the basis of the γ-γ-coincidence data and γ-ray intensities, the 324 and 467 keV transitions are assigned to the de-excitation of the 2_1^+ and 4_1^+ states in ^{196}Os, respectively. The location of these states at 324 and 791 keV agrees with the previous observation of two states at 300 (20) and 760 (20) keV [8]. For the 639 keV transition, two different placements in the level scheme are possible. Its energy corresponds to the value expected from systematics for both the $6_1^+ \rightarrow 4_1^+$ and $2_2^+ \rightarrow 0_{g.s.}^+$ transitions.
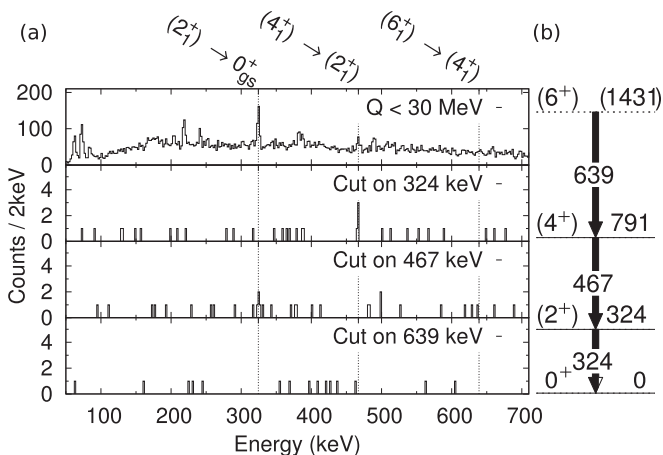
For ^{198}Os only the 2_2^+ to the 2_1^+ transition was observed. In ^{194}Os the 2_2^+ state has been identified which decays to both the 2_1^+ and 0_{gs}^+ states with the former transition having almost twice the intensity. A similar situation in ^{196}Os would lead to the presence of a strong 314.8 keV transition from the 2_2^+ to the 2_1^+ state, which is not observed in our data. However, it is known from experience with multinucleon transfer reactions that the population of a non-yrast 2^+ state is very weak (a few percent of the first 2^+) whereas that of a yrast 6_1^+ state is usually much larger.

Therefore, the assignment of the 639 keV transition to the de-excitation of the 6_1^+ state is favored. The fact that the 639 keV transition does not appear in coincidence with the 324 and 467 keV transitions is most plausible due to the low statistics. In the projection shown in Fig. 2(a) the intensities of the three relevant transitions, although still compatible, because of the large errors, with those of the singles spectrum of Fig. 1(c), have different absolute values, with the 639 keV transition resulting more than three times weaker with respect to the 467 keV one. Considering the number of counts of the 324 and 467 keV peaks in the projection, the expected number of counts in coincidence between them taking into account the quoted efficiency of the AGATA demonstrator is 3, which indeed is what is observed in the two middle spectra of Fig. 2(a). Accordingly, we expect for the 639 keV transition at most one event in coincidence with the 324 and 467 keV lines. This is just at the level of the background observed in our coincidence spectra of Fig. 2(a). In conclusion, the present low-statistics data, although not able to confirm the presence of a 639 keV transition feeding the 4_1^+ state, are compatible with this assumption. The results are summarized in Table I and the proposed level scheme is shown in Fig. 2(b).

In these data, no delayed γ rays for ^{196}Os were observed. Either no isomeric state in ^{196}Os was populated in this experiment or the half-life is outside of the sensitivity of the experimental setup ($\lesssim 8$ or $\gtrsim 400$ ns).

For comparison with the experimental results, state-of-the-art beyond-mean-field calculations have been performed. In this approach, the nuclear states are obtained, using the generator coordinate method [26], by mixing particle number and angular-momentum-projected intrinsic states that have different quadrupole deformations. The latter states are found by the minimization of the particle-number-projected energy (particle number variation after projection method, PN-VAP) [27]. Since triaxial shapes are expected to be relevant in this region, both axial and triaxial deformations (β_2, γ) are considered (see Refs. [28,29] for details). The underlying interaction is chosen to be Gogny D1S [30], which has proven to give a reliable description of many observables and phenomena across the whole nuclear chart [31]. Due to the large computational requirements of these calculations, the number of major oscillator shells included is restricted to 9 and the number of intrinsic states in the generator coordinate method calculation is 60 in a range of $\beta_2 \in [0.0, 0.5]$. In addition, neither time-reversal nor parity-symmetry breaking are included.

Since the quadrupole moment is not a directly observable quantity, the shape evolution can be analyzed by investigating
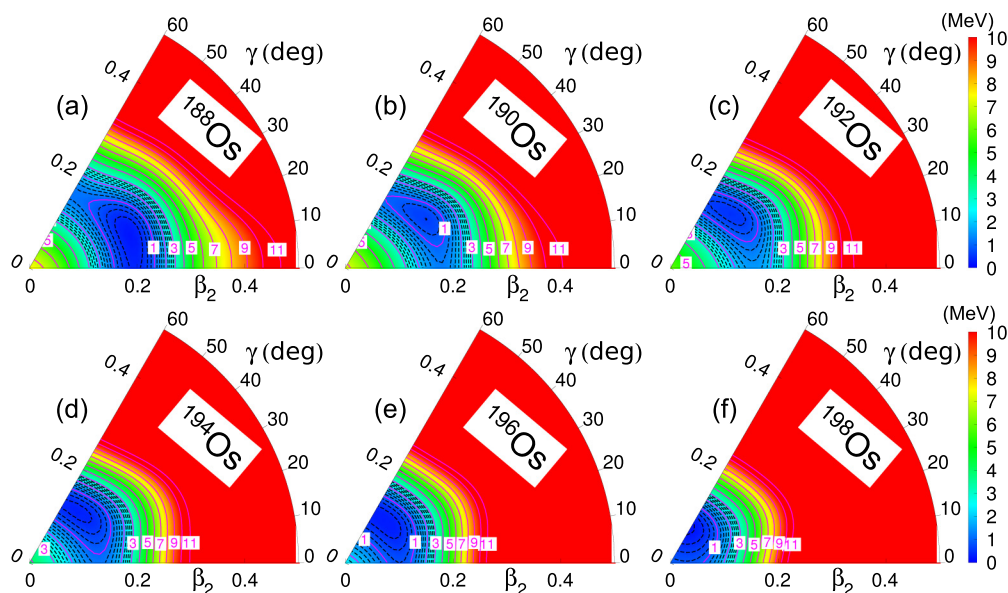
FIG. 2. (a) γ-ray spectrum obtained for ^{196}Os after gating on the beam-like recoils ^{84}Kr having a reconstructed Q value smaller than 30 MeV and with a gate on the γ rays at 324, 467, and 639 keV. (b) Level scheme proposed for ^{196}Os.

FIG. 3. (Color online) Particle number projected potential energy surfaces in the triaxial plane for $^{188-198}$Os isotopes calculated with the Gogny D1S interaction. Solid and dashed contour lines are separated 1.0 and 0.2 MeV, respectively. The solid contour lines are labeled with their energies.

the intrinsic states in terms of the potential energy surface (PES) of each nucleus. In Fig. 3 the PES in the (β_2,γ) plane for $^{188-198}$Os obtained in the PN-VAP approach are shown. Here, a shape transition from a prolate ($\gamma = 0°$) to an oblate ($\gamma = 60°$) minimum is clearly found. Hence, while ^{188}Os has a prolate minimum, the $^{194-198}$Os isotopes are oblate

deformed and ^{190,192}Os are transitional nuclei with triaxial minima at $\gamma \approx 30°$ and $\gamma \approx 45°$, respectively. Nevertheless, a degeneracy is observed in the γ direction, particularly important for the isotopes $^{188-194}$Os, revealing the relevance of this degree of freedom in this region [6,7,35–37]. Additionally, a general reduction in deformation at the minimum of each PES
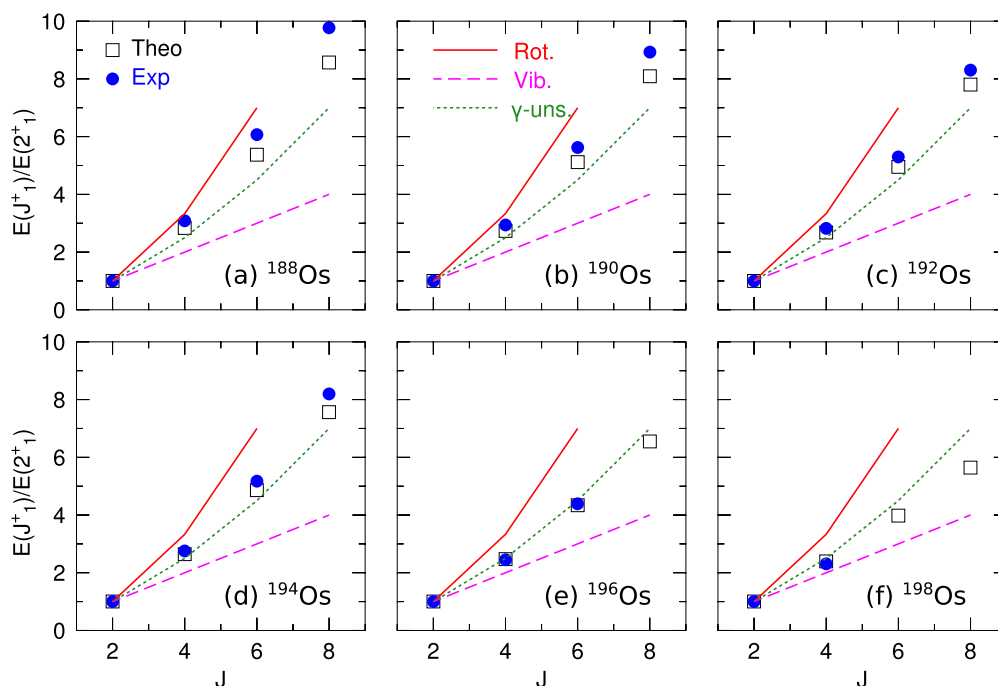

FIG. 4. (Color online) Yrast band excitation energies, normalized to the corresponding 2^+_1 energies, for $^{188-198}$Os isotopes. Blue dots and black boxes are the experimental points and theoretical beyond-mean-field predictions, respectively. Theoretical limits for axial rotor (red continuous line), vibrator (magenta dashed line), and γ-unstable/triaxial rotor (green dotted line) geometrical models are also given. The experimental data are taken from [9,11,32–34] and this work for ^{196}Os.

is observed when neutrons are added, from $\beta_2 = 0.20$ (^{188}Os) to $\beta_2 = 0.07$ (^{198}Os).

The underlying structure of the PES described above is then reflected in the spectra calculated from configuration mixing calculations based on these surfaces. Figure 4 shows the experimental and theoretical $E(J_i^+)/E(2_1^+)$ ratios for the yrast band, compared to the prediction given by axial rotor, γ-unstable/triaxial rotor, and vibrator limits [38]. The experimental spectra are close to the γ-unstable/triaxial rotor limit for most of the isotopes analyzed here. However, a smooth transition from a more axial rotational behavior in ^{188}Os through triaxial configurations towards more vibrational spectra in ^{198}Os can be observed when pairs of neutrons are added. An almost perfect γ-unstable/triaxial rotor yrast band is predicted for ^{196}Os in agreement with the experimental ratio $E(4_1^+)/E(2_1^+)$ and also with the assumption of the 639 keV transition as the γ ray corresponding to the transition $(6_1^+) \rightarrow (4_1^+)$ [see Fig. 4(e)]. For the remaining isotopes, the agreement between the theoretical predictions and the available experimental data is also good, although $^{188-194}$Os are predicted to be more γ-unstable/triaxial rotors than the actual experimental values, which are slightly more axial rotor-like. These results give confidence to the description of the shape transition from prolate/γ-soft to slightly oblate/γ-soft nuclei found in Fig. 3 for this isotopic chain.

In summary, the γ rays from the two lowest-lying yrast states of the neutron-rich isotope ^{196}Os have been observed for the first time, using a multinucleon transfer reaction from the ^{198}Pt target to the ^{82}Se beam. An additional γ ray with an energy of 639 keV was found and could originate from the de-excitation of the 6_1^+ state. State-of-the-art beyond-mean-field calculations were performed for the even-even $^{188-198}$Os isotopes. The predictions suggest a smooth transition in the Os isotopes from a more axial rotational behavior towards predominately vibrational nuclei passing through a γ-soft configuration. The predicted low-lying excited states for the even-even $^{188-198}$Os agree well with the experimental data. In particular, the newly measured yrast band in ^{196}Os that exhibits an almost perfect γ-unstable/triaxial character is accurately reproduced. Further experimental work to determine the γ-band, lifetimes of the low-lying states, quadrupole moments, etc., will help to further elucidate the nature of ^{196}Os.

[1] R. F. Casten, Nat. Phys. **2**, 811 (2006).
[2] I. Hamamoto and B. R. Mottelson, Phys. Rev. C **79**, 034317 (2009).
[3] R. Bengtsson *et al.*, Phys. Lett. B **183**, 1 (1987).
[4] L. M. Robledo *et al.*, J. Phys. G **36**, 115104 (2009).
[5] A. Ansari, Phys. Rev. C **33**, 321 (1986).
[6] P. Sarriguren, R. Rodríguez-Guzmán, and L. M. Robledo, Phys. Rev. C **77**, 064322 (2008).
[7] K. Nomura, T. Otsuka, R. Rodríguez-Guzmán, L. M. Robledo, and P. Sarriguren, Phys. Rev. C **84**, 054316 (2011).
[8] P. D. Bond *et al.*, Phys. Lett. B **130**, 167 (1983).
[9] C. Wheldon *et al.*, Phys. Rev. C **63**, 011304 (2000).
[10] J. J. Valiente-Dobón *et al.*, in *Nuclear Physics, Large and Small: International Conference on Microscopic Studies of Collective Phenomena*, edited by R. Bijker, A. Frank, and R. F. Casten, AIP Conference Proceedings Vol. 726 (AIP, New York, 2004), p. 249.
[11] Zs. Podolyák *et al.*, Phys. Rev. C **79**, 031305 (2009).
[12] Zs. Podolyák *et al.*, Phys. Lett. B **491**, 225 (2000).
[13] G. D. Dracoulis *et al.*, in *Journal of Physics: Conference Series*, Vol. 381 (IOP, Bristol, UK, 2012), p. 012060.
[14] G. D. Dracoulis *et al.*, Phys. Lett. B **720**, 330 (2013).
[15] R. F. Casten *et al.*, Phys. Lett. B **76**, 280 (1978).
[16] S. J. Steer *et al.*, Phys. Rev. C **84**, 044313 (2011).
[17] M. Caamaño *et al.*, Eur. Phys. J. A **23**, 201 (2005).
[18] P.-A. Söderström *et al.*, Phys. Rev. C **81**, 034310 (2010).
[19] A. Gadea *et al.*, Nucl. Instrum. Methods Phys. Res. A **654**, 88 (2011).
[20] S. Akkoyun *et al.*, Nucl. Instrum. Methods Phys. Res. A **668**, 26 (2012).
[21] A. M. Stefanini *et al.*, Nucl. Phys. A **701**, 217 (2002).
[22] S. Szilner *et al.*, Phys. Rev. C **76**, 024604 (2007).
[23] D. Montanari *et al.*, Eur. Phys. J. A **47**, 4 (2011).
[24] A. Lopez-Martens *et al.*, Nucl. Instrum. Methods Phys. Res. A **533**, 454 (2004).
[25] L. C. Northcliffe and R. F. Schilling, At. Data Nucl. Data Tables **7**, 233 (1970).
[26] P. Ring and P. Schuck, *The Nuclear Many-Body Problem* (Springer, New York, 2004).
[27] M. Anguiano *et al.*, Nucl. Phys. A **696**, 467 (2001).
[28] T. R. Rodríguez and J. L. Egido, Phys. Rev. C **81**, 064323 (2010).
[29] M. Bender and P.-H. Heenen, Phys. Rev. C **78**, 024309 (2008).
[30] J. F. Berger *et al.*, Nucl. Phys. A **428**, 23 (1984).
[31] J. P. Delaroche *et al.*, Phys. Rev. C **81**, 014303 (2010).
[32] B. Singh, Nucl. Data Sheets **95**, 387 (2002).
[33] B. Singh, Nucl. Data Sheets **99**, 275 (2003).
[34] C. M. Baglin, Nucl. Data Sheets **113**, 1871 (2012).
[35] P. Möller, R. Bengtsson, B. G. Carlsson, P. Olivius, and T. Ichikawa, Phys. Rev. Lett. **97**, 162502 (2006).
[36] K. Heyde and J. L. Wood, Rev. Mod. Phys. **83**, 1467 (2011).
[37] T. Nikšić, P. Ring, D. Vretenar, Y. Tian, and Z.-y. Ma, Phys. Rev. C **81**, 054318 (2010).
[38] J. Zhang *et al.*, Phys. Lett. B **407**, 201 (1997).